

Fast adaptive and selective mean filter for the removal of high-density salt and pepper noise

ISSN 1751-9659
 Received on 1st March 2017
 Revised 13th February 2018
 Accepted on 16th March 2018
 E-First on 19th April 2018
 doi: 10.1049/iet-ipr.2017.0199
www.ietdl.org

Samsad Beagum Sheik Fareed¹✉, Sheeja Shaik Khader²

¹Department of Computer Science, Karpagam University, Karpagam Academy of Higher Education, Coimbatore, India

²Department of Computer Applications, Karpagam University, Karpagam Academy of Higher Education, Coimbatore, India

✉ E-mail: samsad.beagum@gmail.com

Abstract: A fast adaptive and selective mean filter is presented to remove salt and pepper noise effectively from images corrupted with higher noise densities. The algorithm achieves better results in terms of visual quality and in terms of peak signal-to-noise ratio, mean absolute error, mean structural similarity index measure, image enhancement factor, and edge preservation ratio than many existing state-of-the-art algorithms at all noise densities. Adaptive filters that use variable window size produce better restoration of salt and pepper noise at higher noise densities than filters that use fixed window size, but they consume more time. This makes them practically impossible to implement them in digital image acquisition devices. Hence, reducing the execution time of adaptive filters is vital. The proposed algorithm consumes around 90% less time for lower noise densities and 50% less time for higher noise densities than the adaptive weighted mean filter, one of the best available adaptive filters in the literature for high-density salt and pepper noise removal.

1 Introduction

Salt and pepper noise appears in digital images due to hot pixels caused by leakage of current in image sensors [1]. Digital cameras use a technique called dark frame subtraction that needs a mechanical shutter to remove salt and pepper noise from captured images. Many devices like cell phone cameras do not have a mechanical shutter and hence require fast and efficient algorithms to remove salt and pepper noise. Median filters are predominantly used to remove salt and pepper noise. The standard median filter (SMF) [2], switching median filters [3, 4], adaptive median filter (AMF) [5], and adaptive centre weighted median filter (ACWMF) [6] are effective in removing salt and pepper noise at lower densities, but they fail to remove noise effectively at higher densities.

Various median filters exist in the literature to remove salt and pepper noise at higher densities [7–19]. Several other filters that use different methodologies have also been proposed [20–25] for removing high-density salt and pepper noise. Wang *et al.* [20] have proposed the use of fuzzy logic and weighted mean filtering for removing salt and pepper noise. Wang *et al.* [21] have presented an impulse noise removal method based on non-uniform sampling and supervised piecewise autoregressive modelling and Roig and Estruch [22] have proposed a vector filter based on geometric information, for removing high-density salt and pepper noise. Lin *et al.* [23] have proposed a mean filter based on morphological image processing and Chen *et al.* [24] have proposed a sparse representation model, for removing high-density salt and pepper noise. Bai and Tan [25] have presented a filter that uses local mean and variance to detect noisy pixels and Newton–Thiele filter to restore the noisy pixels.

In this paper, the performance of the various median filters used in removing salt and pepper noise is analysed. Most of the median filters [7–19] in the literature work in two stages. The first stage detects the noisy pixels, while the second stage restores the identified noisy pixels. Decision-based algorithm (DBA) [7] is a very fast 3×3 selective median filter that replaces the noisy pixels with the median of the noise-free pixels in the filtering window and if there are no noise-free pixels, it uses the previously processed noise-free pixel for replacement. However, DBA produces stripes in restored images. Unsymmetric trimmed median filter (UTMF) [8] is introduced as an improvement to DBA to remove the stripes

in restored images. It simply does nothing when there are no noise-free pixels. Modified decision-based unsymmetric trimmed median filter (MDBUTMF) [9] is then introduced as an improvement to UTMF that replaces the noisy pixels with the mean of the 3×3 filter when there are no noise-free pixels. Both UTMF and MDBUTMF remove the striped effect, but still they fail to restore images effectively at noise densities $>70\%$. The two variants of MDBUTMF, namely MDBUTMF_2 [10] and MDBUTMF_3 [11], interestingly produce similar but better results than MDBUTMF at higher noise ratios. MDBUTMF_2 uses the mean of the noise-free pixels instead of the median, whereas MDBUTMF_3 uses two iterations of MDBUTMF. The results of these algorithms show that mean filtering performs better than median filtering for higher noise densities. One of the important factors behind the fast execution of these 3×3 filters is their simple impulse detection procedure that detects the minimum and maximum grey-level values used by the image as noisy.

Adaptive filters that increase the window size during filtering have also been proposed for high-density salt and pepper noise removal. Adaptive filters begin filtering with a 3×3 filtering window. If the condition specific to the adaptive filter is not satisfied by the pixels in the current filtering window, the adaptive filter increases the size of the filtering window usually by 2 and applies the filtering condition in the new window. This process is repeated either until the condition is met or until a predefined maximum window size is reached.

Ibrahim *et al.* [12] have introduced an AMF (AMF_Haidi) that adaptively increases the window size until eight noise-free pixels are found. Then the noisy pixel is replaced by the median of the noise-free pixels. AMF_Haidi gives better results than DBA, MDBUTMF, and its variants, but it takes more time than they do. AMF_Haidi also uses the simple impulse detection procedure used by DBA and MDBUTMF variants.

Adaptive weighted mean filter (AWMF) [13] is an adaptive filter that identifies a pixel as noisy if its grey level does not lie between the minimum and maximum grey levels of the filtering window. It replaces a noisy pixel with the mean of the noise-free pixels in the filtering window. If there are no noise-free pixels in the filtering window, it increases the size of the filtering window. In addition, while processing a noisy pixel, if the minimum and maximum values of two successive filtering windows are same, the algorithm stops increasing the window size further to save time. It

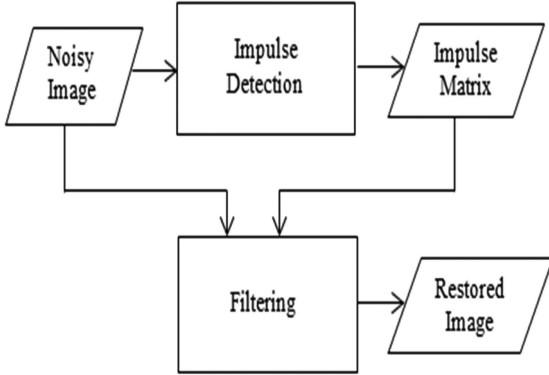


Fig. 1 Two stages of the proposed algorithm

0	0	255	0	255
255	0	0	255	255
54	64	255	65	25
32	255	0	255	0
90	90	32	55	65

Fig. 2 5×5 filtering window

is found that AWMF gives better results than AMF_Haidi and all the other filters discussed above for higher noise densities which makes it the best filter available for salt and pepper noise removal, but it consumes more time than all the other filters. The restoration results given by AWMF again show that mean filtering performs better than median filtering to remove high-density salt and pepper noise. In addition, it is noted that adaptive filters produce better results than filters using fixed window size at higher noise densities, but they consume more time, making it impractical to implement them in image acquisition devices.

In this paper, all the best strategies that yield better high-density salt and pepper noise removal are combined to produce a fast adaptive and selective mean filter. It achieves better results than all the adaptive filters, including the AWMF at all noise densities and consumes less than half of the time taken by the adaptive filters including the AWMF at higher noise densities. At lower noise densities, it takes around 90% less time than AWMF, providing a significant improvement in execution time. The proposed method is explained in Section 2. Section 3 discusses the experimental results and the conclusion is presented in Section 4.

2 Proposed method

The proposed method works in two stages, (i) the impulse detection stage and (ii) the restoration stage as shown in Fig. 1.

2.1 Impulse detection stage

Like any switching filter [3, 4, 6, 8], the impulse detection stage identifies the noisy pixels in the noisy image and produces an impulse matrix as output. The impulse matrix has a value 1 if the corresponding pixel in the noisy image is noisy, otherwise its value is 0. If Org denotes an original noise-free image, then a pixel in the noisy image X corrupted with $p = p_{\min} + p_{\max}$ salt and pepper noise may have a grey level as follows:

$$X(i, j) = \begin{cases} \text{imp}_{\min}, & \text{with probability } p_{\min}, \\ \text{imp}_{\max}, & \text{with probability } p_{\max}, \\ \text{Org}(i, j), & \text{with probability } 1 - (p_{\min} + p_{\max}) \end{cases} \quad (1)$$

where imp_{\min} and imp_{\max} are the minimum and maximum grey-level values used by the salt and pepper noise model. For an image whose pixel values range between 0 and 255, $\text{imp}_{\min} = 0$ and $\text{imp}_{\max} = 255$.

The impulse detection stage of the proposed method uses the simple procedure of marking the pixels with values imp_{\min} or imp_{\max} as noisy. If isImp denotes the impulse matrix output by the impulse detection stage, then

$$\text{isImp}(i, j) = \begin{cases} 1, & \text{if } X(i, j) = \text{imp}_{\min} \text{ or} \\ & X(i, j) = \text{imp}_{\max} \\ 0, & \text{otherwise} \end{cases} \quad (2)$$

2.2 Restoration stage

The restoration stage processes only the pixels identified as noisy in the first stage. If X_{noisy} denotes the set of pixels identified as noisy in the first stage, then X_{noisy} is given by

$$X_{\text{noisy}} = \{x(i, j) \in X \mid \text{isImp}(i, j) = 1\} \quad (3)$$

From the analysis of the results given by the various filters discussed in Section 1, it is found that mean filtering performs better than median filtering in restoring high-density salt and pepper noise and adaptive filters perform better than filters with fixed window size. Hence, to restore the noisy pixels, the proposed method uses a selective mean filter with adaptive window size where the window size can be increased during the spatial processing. The selective mean filter selects only the noise-free pixels in the filtering window for calculating the mean.

For each pixel identified as noisy in the impulse detection stage, the restoration stage counts the number of noise-free pixels in its 3×3 neighbourhood. If it finds at least a minimum of one or two noise-free pixels in the current neighbourhood, it replaces the noisy pixel with the mean of those nearest noise-free pixels. If it does not find any noise-free pixel in the current neighbourhood, it increases the window size by 2 and repeats the restoration steps again.

The proposed restoration technique gives higher priority to only those noise-free pixels that are nearer to the noisy pixel, i.e. those pixels that have a shorter D8 or chessboard distance from the noisy pixel are used in restoration. The D8 or chessboard distance between two pixels at positions (x_1, y_1) and (x_2, y_2) is given by the following equation

$$\text{D8 distance} = \max(|x_2 - x_1|, |y_2 - y_1|) \quad (4)$$

For example in the 5×5 neighbourhood shown in Fig. 2, the noise-free pixels are shown in italics. There are two noise-free pixels in D8 distance = 1 and there are eight noise-free pixels in D8 distance = 2 from the centre pixel. The proposed technique uses only the two noise-free pixels in D8 distance = 1 in the restoration procedure. The mean of the nearest two noise-free pixels in the 3×3 neighbourhood can yield better restoration than the mean of the ten noise-free pixels in the 5×5 neighbourhood which may result in blurring.

Let the variable SelCount refer to the number of nearest noise-free pixels used to determine the adaptive window size in the restoration procedure. If F_w denotes the filtering window of the noisy image, Imp_w denotes the corresponding pixels in the impulse matrix isImp , $W_s \times W_s$ denotes the size of F_w , and $W_{s\max} = 39$ denotes the maximum window size used by the proposed algorithm, then for each noisy pixel $X_{\text{noisy}}(i, j)$ in the noisy image X , the simple restoration procedure works as follows.

Step 1: Set the initial filtering window size $W_s = 3$.

Step 2: Count the number of noise-free pixels NF_{count} in the $W_s \times W_s$ filtering window F_w .

Step 3: If $\text{NF}_{\text{count}} \geq \text{SelCount}$, then replace the noisy pixel with the mean of the noise-free pixels in the filtering window and go to step 6.

Step 4: If $\text{NF}_{\text{count}} < \text{SelCount}$, then increase the window size W_s by 2 and go to step 2.

Step 5: If the filtering window size $W_s > W_{s\max}$, then replace the noisy pixel with the mean of the filtering window and go to step 6.

Step 6: Process the next noisy pixel.

The restoration procedure is summarised in (5)–(7). If \mathbf{NF} denotes the set of noise-free pixels in the filtering window F_w with initial window size $W_s = 3$, then \mathbf{NF} is given by

$$\mathbf{NF} = \{nf(i, j) \in F_w | \text{isImp}(u, v) = 0, i = u, j = v\} \quad (5)$$

The number of noise-free pixels NF_{count} is given by

$$NF_{\text{count}} = \text{sizeof}(\mathbf{NF}) \quad (6)$$

The restored value of the noisy pixel $X_{\text{noisy}}(i, j)$ is given by the function $f(W_s)$ as

$$f(W_s) = \begin{cases} \text{mean}(\mathbf{NF}), & NF_{\text{count}} \geq SelCount \\ \text{mean}(F_w), & W_s > W_{\text{smax}} \\ f(W_s + 2), & \text{Otherwise} \end{cases} \quad (7)$$

The proposed algorithm (Fig. 3) gives best results for values of 1 and 2 for the variable SelCount. It shows that the mean of the noise-free neighbours in the nearest neighbourhood yield better restoration. The maximum value of W_s reached is 13, i.e. at least two noise-free pixels are found within a window size of 13×13 for all test images at all noise densities. However, for images with numerous black and white pixels like X-ray images, the maximum window size W_{smax} is reached.

3 Experimental results

The proposed algorithm with $SelCount = 2$ is denoted by PA1 and $SelCount = 1$ is denoted by PA2 in the following discussions. The PA1 and PA2 are tested with all the standard grey-scale images of size 512×512 from Gonzalez and Woods book of Digital Image processing [26]. The standard grey-scale images include Lena, Camera-man, Bridge, Living-room, Mandril, House, Jetplane, Lake, Peppers, Pirate, WomanBlondeHair, and WomanDarkHair. The proposed methods are also tested with X-ray images from Medpix [27] to analyse their performance in the presence of numerous black and white pixels. PA1 and PA2 are compared with several existing algorithms including SMF, ACWMF, AMF, progressive switching median filter (PSMF), DBA, UTMF, MDBUTMF, MDBUTMF_2, MDBUTMF_3, AMF_Haidi, and AWMF. All the algorithms are implemented in 64 bit MATLAB R2015a in a computer having Intel Core I5 processor with speed 2.30 GHz and 6 GB RAM.

The measures used for comparison are peak signal-to-noise ratio (PSNR), mean absolute error (MAE), image enhancement factor (IEF), mean structural similarity index measure (MSSIM), and edge preservation ratio [28] in terms of accuracy (EPRa) and robustness (EPRr) given by

$$\text{PSNR} = 10 \log_{10} \frac{255^2}{(\text{Rows} \times \text{Cols}) \sum_{i,j} (R(i, j) - O(i, j))^2} \quad (8)$$

$$\text{MAE} = \frac{1}{\text{Rows} \times \text{Cols}} \sum_{i,j} |R(i, j) - O(i, j)| \quad (9)$$

$$\text{IEF} = \frac{\sum_{i,j} (X(i, j) - O(i, j))^2}{\sum_{i,j} (R(i, j) - O(i, j))^2} \quad (10)$$

$$\text{MSSIM}(\mathbf{O}, \mathbf{R}) = \frac{1}{\text{NW}} \sum_i \text{SSIM}(\mathbf{o}_i, \mathbf{r}_i) \quad (11)$$

where \mathbf{O} , \mathbf{X} , and \mathbf{R} are the original, corrupted, and restored images, respectively; Rows \times Cols give the size of the image; NW is the number of windows used in MSSIM calculation; \mathbf{o}_i and \mathbf{r}_i are the portions of the original and restored images at window i ; and

(F_w denotes the filtering window; \tilde{I}_{imp_w} denotes the corresponding values in the impulse matrix)

```

for each  $X(i, j)$ 
  if  $\text{isImp}(i, j) == 1$ 
     $W_s = 3;$ 
    loop
     $NF_{\text{count}} = 0;$ 
    for each  $\text{isImp}(i + \Delta i, j + \Delta j) \in \tilde{I}_{\text{imp}_w}$ 
      if  $\text{isImp}(i + \Delta i, j + \Delta j) == 0,$ 
         $NF_{\text{count}} = NF_{\text{count}} + 1;$ 
    end for
    if  $NF_{\text{count}} \geq SelCount,$ 
       $X(i, j) = \text{mean}(X(i + \Delta i, j + \Delta j))$ 
      |  $X(i + \Delta i, j + \Delta j) \in F_w \wedge$ 
         $\text{isImp}(i + \Delta i, j + \Delta j) = 0;$ 
      break;
    else if  $NF_{\text{count}} < SelCount,$ 
       $W_s = W_s + 2;$ 
      if  $W_s > W_{\text{smax}},$ 
         $X_{\text{noisy}}(i, j) = \text{mean}(X(i, j)) \mid X(i, j) \in F_w;$ 
        break;
      end if
    end if
  end loop
end if
end for

```

Fig. 3 Algorithm: Restoration procedure of the proposed algorithm

$$\text{SSIM}(\mathbf{o}, \mathbf{r}) = \frac{(2 \times \text{avg}(\mathbf{o}) \times \text{avg}(\mathbf{r}) + C_1)(2 \times \text{cov}(\mathbf{o}, \mathbf{r}) + C_2)}{(\text{avg}(\mathbf{o})^2 + \text{avg}(\mathbf{r})^2 + C_1)(\sigma^2(\mathbf{o}) + \sigma^2(\mathbf{r}) + C_2)} \quad (12)$$

where avg refers to average, σ^2 the variance, and cov the covariance; $C_1 = (0.01 \times \text{imp}_{\text{max}})^2$ and $C_2 = (0.03 \times \text{imp}_{\text{max}})^2$ by default

$$\text{EPRa} = \frac{\text{EPnts}_o \cap \text{EPnts}_r}{\text{EPnts}_o} \quad (13)$$

$$\text{EPRr} = \frac{\text{EPnts}_o \cap \text{EPnts}_r}{\text{EPnts}_o \cup \text{EPnts}_r} \quad (14)$$

where EPnts_o and EPnts_r are the edge points extracted from the original image and the restored image, respectively, using the Canny edge detector with a high threshold of 0.1 for strong edges and a low threshold of 0.04 for weak edges.

Fig. 4 shows the comparative performance of PA1 and PA2 in terms of PSNR, MAE, MSSIM, and IEF measures for the Lena image at higher noise densities ranging around 40–90%. It is found that PA1 gives better PSNR, MAE, and IEF results than PA2 for all tested images. However, PA2 gives better MSSIM score and visual quality than PA1. For lower noise ratios, the measures remained same for both PA1 and PA2.

Figs. 5–7 show the Lena images restored by the various filters at 90% salt and pepper noise. Figs. 8–10 show the Camera-man images restored by the various filters at 80% salt and pepper noise. It is found that PA2 produces better visual quality images than all the other filters even at 90% noise ratio. When comparing the images restored by PA1 and PA2, they show similar visual quality until 70%, whereas >70% PA2 produced slightly sharper images than PA1.

Tables 1 and 2 show the IEF and PSNR results given by the various filters for the test images corrupted with 90% noise density. The values show that PA1 gives better IEF and PSNR measures than all the other filters, whereas PA2 gives similar measures as AWMF.

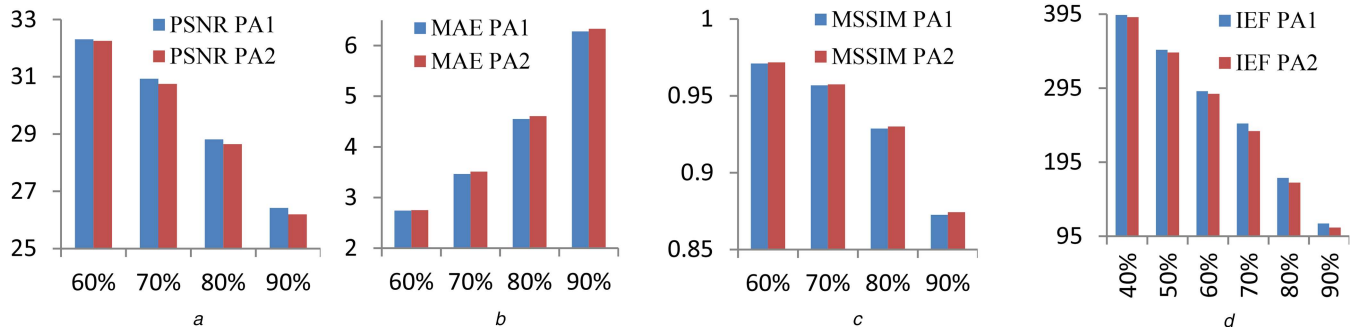


Fig. 4 Results for Lena image by PA1 and PA2 at higher noise densities
(a) PSNR, (b) MAE, (c) MSSIM, (d) IEF

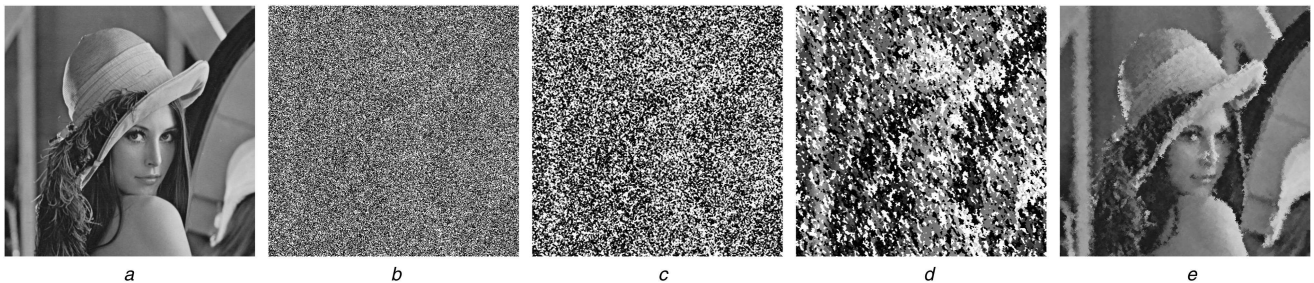


Fig. 5 Restored images of Lena at 90% salt and pepper noise by various filters – part 1
(a) Original image, (b) Image with 90% salt and pepper noise. Image restored by, (c) SMF, (d) ACWMF, (e) AMF

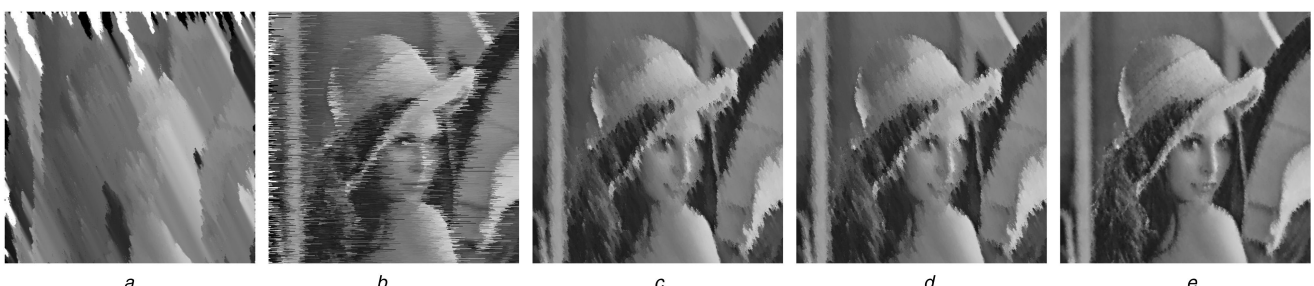


Fig. 6 Restored images of Lena at 90% salt and pepper noise by various filters – part 2
(a) PSMF, (b) DBA, (c) UTMF, (d) MDBUTMF, (e) MDBUTMF_2



Fig. 7 Restored images of Lena at 90% salt and pepper noise by various filters – part 3
(a) MDBUTMF_3, (b) AMF_Haidi, (c) AWMF, (d) PA1, (e) PA2

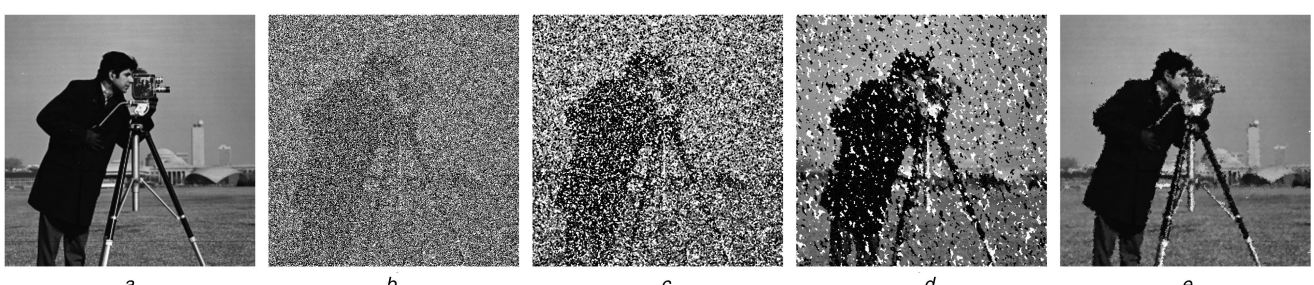


Fig. 8 Restored images of Camera-man at 80% salt and pepper noise by various filters – part 1
(a) Original image, (b) Image with 80% salt and pepper noise. Image restored by, (c) SMF, (d) ACWMF, (e) AMF

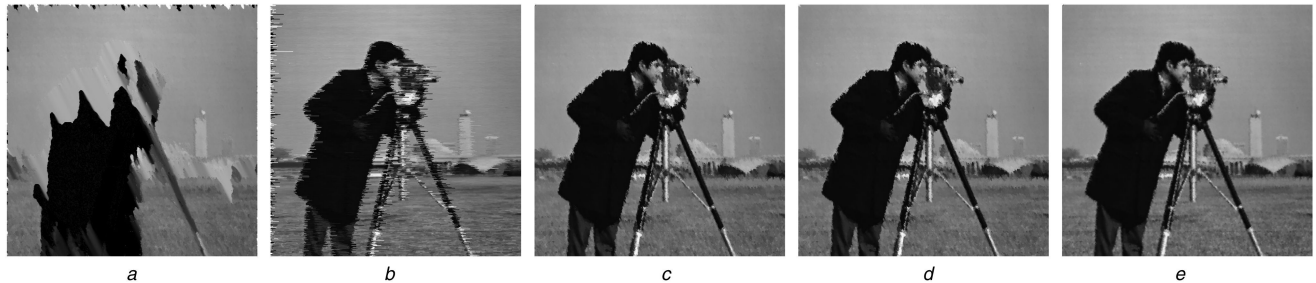


Fig. 9 Restored images of Camera-man at 80% salt and pepper noise by various filters – part 2
(a) PSMF, (b) DBA, (c) UTMF, (d) MDBUTMF, (e) MDBUTMF_2

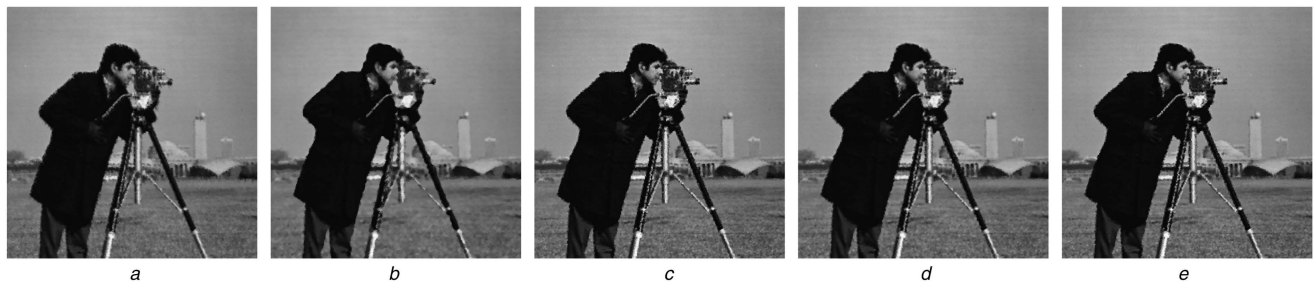


Fig. 10 Restored images of Camera-man at 80% salt and pepper noise by various filters – part 3
(a) MDBUTMF_3, (b) AMF_Haidi, (c) AWMF, (d) PA1, (e) PA2

Table 1 IEF results for various images at 90% noise density

	Lena	Bridge	Camera-man	Living-Room	Mandrill	House	JetPlane	Lake	Peppers	Pirate	Woman-Blonde	Woman-DarkHair
SMF	1.19	1.18	1.18	1.19	1.18	1.19	1.19	1.18	1.18	1.19	1.18	1.18
ACWMF	2.06	1.84	1.92	1.96	1.94	1.90	1.86	1.81	1.91	1.89	2.00	1.93
AMF	41.92	18.96	33.64	27.37	21.00	66.13	34.70	23.91	39.89	33.64	34.68	111.19
PSMF	4.92	4.24	3.26	5.92	4.98	3.45	5.33	3.33	3.97	4.64	6.20	2.82
DBA	10.26	11.23	11.06	13.20	11.03	15.02	13.47	9.34	10.57	11.86	12.51	19.28
UTMF	26.11	16.17	22.74	22.94	23.87	29.33	21.97	16.58	21.35	23.25	25.84	45.20
MDBUTMF	26.11	16.17	22.74	22.94	23.89	29.33	21.97	16.58	21.34	23.27	25.84	45.20
MDBUTMF_2	61.39	27.64	50.23	42.30	35.54	73.38	46.27	33.91	52.58	48.97	48.11	132.01
MDBUTMF_3	61.39	27.64	50.24	42.32	35.54	29.34	21.97	16.58	21.35	23.26	25.84	45.20
AMF_Haidi	86.00	32.89	57.83	45.70	33.07	152.84	58.36	43.79	89.07	64.19	55.03	316.72
AWMF	106.63	36.02	90.71	54.35	38.70	255.97	86.14	58.12	106.39	73.52	62.87	426.38
PA1	112.26	38.94	90.05	57.50	39.95	257.94	86.70	61.16	115.72	79.49	68.52	463.86
PA2	106.71	36.03	90.81	54.37	38.73	256.13	86.22	58.16	106.41	73.50	62.86	426.92

Table 2 PSNR results for various images at 90% noise density

	Lena	Bridge	Camera-man	Living-Room	Mandrill	House	JetPlane	Lake	Peppers	Pirate	Woman-Blonde	Woman-DarkHair
SMF	6.68	6.40	6.25	6.74	6.81	6.42	6.11	6.19	6.47	6.59	6.73	6.20
ACWMF	9.05	8.34	8.38	8.91	8.95	8.46	8.08	8.03	8.54	8.61	9.03	8.33
AMF	22.14	18.48	20.80	20.35	19.30	23.86	20.78	19.24	21.75	21.12	21.41	25.93
PSMF	12.83	11.98	10.67	13.70	13.05	11.04	12.64	10.69	11.73	12.52	13.93	9.97
DBA	16.03	16.20	15.97	17.19	16.50	17.43	16.67	15.16	15.98	16.59	16.98	18.32
UTMF	20.08	17.79	19.10	19.59	19.86	20.33	18.79	17.65	19.03	19.51	20.13	22.02
MDBUTMF	20.08	17.79	19.10	19.59	19.86	20.33	18.79	17.65	19.03	19.52	20.13	22.02
MDBUTMF_2	23.80	20.12	22.54	22.24	21.58	24.31	22.03	20.76	22.95	22.75	22.83	26.68
MDBUTMF_3	23.80	20.12	22.54	22.24	21.58	20.33	18.79	17.65	19.03	19.52	20.13	22.02
AMF_Haidi	25.26	20.87	23.15	22.58	21.27	27.50	23.04	21.87	25.24	23.92	23.42	30.48
AWMF	26.19	21.27	25.11	23.33	21.95	29.74	24.73	23.10	26.01	24.51	23.99	31.77
PA1	26.42	21.60	25.08	23.58	22.09	29.77	24.75	23.32	26.37	24.85	24.37	32.14
PA2	26.20	21.27	25.11	23.33	21.96	29.74	24.73	23.10	26.01	24.51	23.99	31.78

Fig. 11 shows the plot of MSSIM values given by the various filters for the various test images. It is found that PA2 gives the best MSSIM measures as AWMF, whereas PA1 gives the second best MSSIM scores.

Tables 3 and 4 show the edge preservation ratio in terms of accuracy EPRA and robustness EPRR given by the various filters for the test images corrupted with 90% noise density. The results show that PA2 and AWMF have higher edge preservation accuracy and

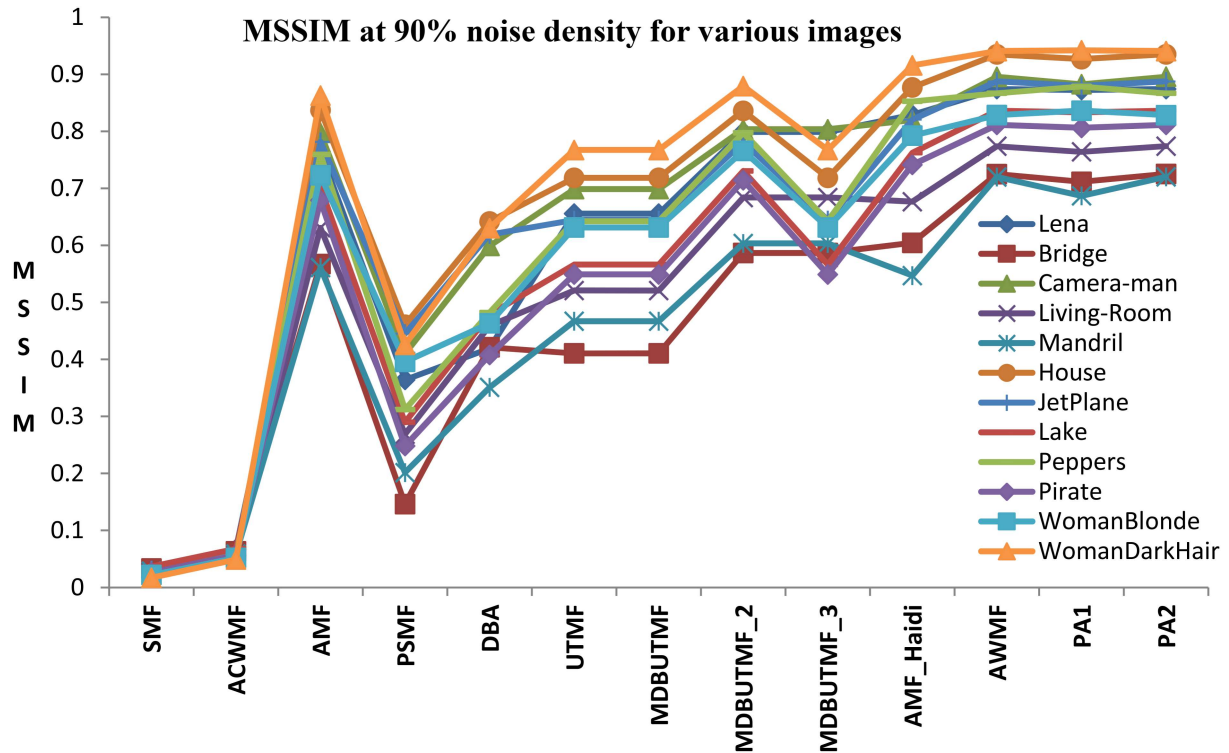


Fig. 11 Plot of MSSIM results given by various filters for images corrupted with 90% noise density

Table 3 EPrA results for various images at 90% noise density

	Lena	Bridge	Camera-man	Living-Room	Mandril	House	JetPlane	Lake	Peppers	Pirate	Woman-Blonde	Woman-DarkHair
SMF	0.314	0.313	0.310	0.313	0.311	0.310	0.311	0.310	0.311	0.312	0.308	0.309
ACWMF	0.232	0.229	0.225	0.233	0.232	0.224	0.232	0.227	0.225	0.236	0.233	0.225
AMF	0.269	0.266	0.262	0.253	0.272	0.207	0.279	0.276	0.267	0.269	0.265	0.226
PSMF	0.022	0.049	0.025	0.027	0.040	0.025	0.023	0.048	0.055	0.045	0.026	0.049
DBA	0.187	0.233	0.229	0.203	0.207	0.141	0.227	0.219	0.194	0.182	0.196	0.166
UTMF	0.169	0.167	0.129	0.171	0.197	0.113	0.181	0.182	0.179	0.164	0.206	0.156
MDBUTMF	0.169	0.167	0.129	0.173	0.209	0.113	0.181	0.182	0.179	0.164	0.206	0.156
MDBUTMF_2	0.255	0.247	0.216	0.256	0.260	0.163	0.256	0.271	0.263	0.257	0.272	0.211
MDBUTMF_3	0.255	0.247	0.216	0.262	0.272	0.113	0.181	0.182	0.179	0.164	0.206	0.156
AMF_Haidi	0.202	0.166	0.155	0.178	0.182	0.170	0.204	0.202	0.237	0.190	0.210	0.187
AWMF	0.379	0.341	0.360	0.356	0.355	0.309	0.377	0.363	0.360	0.364	0.341	0.337
PA1	0.336	0.291	0.303	0.294	0.305	0.269	0.324	0.321	0.323	0.320	0.306	0.286
PA2	0.378	0.342	0.360	0.355	0.356	0.310	0.378	0.365	0.360	0.363	0.342	0.337

Table 4 EPrR results for various images at 90% noise density

	Lena	Bridge	Camera-man	Living-Room	Mandril	House	JetPlane	Lake	Peppers	Pirate	Woman-Blonde	Woman-DarkHair
SMF	0.071	0.147	0.067	0.112	0.161	0.049	0.068	0.086	0.061	0.107	0.079	0.050
ACWMF	0.068	0.126	0.066	0.102	0.137	0.048	0.066	0.081	0.058	0.100	0.076	0.050
AMF	0.147	0.162	0.157	0.146	0.175	0.124	0.159	0.155	0.128	0.156	0.131	0.123
PSMF	0.016	0.042	0.020	0.023	0.036	0.017	0.018	0.037	0.033	0.035	0.020	0.029
DBA	0.075	0.141	0.111	0.113	0.133	0.062	0.114	0.104	0.074	0.096	0.090	0.068
UTMF	0.096	0.110	0.087	0.103	0.138	0.064	0.100	0.106	0.084	0.101	0.108	0.079
MDBUTMF	0.096	0.110	0.087	0.104	0.143	0.064	0.100	0.106	0.084	0.101	0.108	0.079
MDBUTMF_2	0.154	0.157	0.144	0.161	0.178	0.101	0.146	0.159	0.131	0.158	0.146	0.116
MDBUTMF_3	0.154	0.157	0.144	0.163	0.183	0.064	0.100	0.106	0.084	0.101	0.108	0.079
AMF_Haidi	0.140	0.121	0.116	0.124	0.134	0.124	0.141	0.141	0.141	0.137	0.130	0.113
AWMF	0.228	0.217	0.238	0.215	0.235	0.213	0.238	0.220	0.186	0.222	0.189	0.178
PA1	0.211	0.191	0.206	0.187	0.208	0.186	0.208	0.200	0.180	0.205	0.175	0.161
PA2	0.228	0.217	0.238	0.215	0.236	0.214	0.238	0.220	0.186	0.222	0.189	0.178

robustness than all the other filters. PA2 gives the second highest score.

Table 5 shows the PSNR results given by the various filters at all noise densities for the Lena image. The PSNR results obtained

Table 5 PSNR results for the Lena image at all noise densities

Noise, %	SMF	ACWMF	AMF	PSMF	DBA	UTMF	MD BUTMF	MD BUTMF_2	MD BUTMF_3	AMF_Haidi	AWMF	PA1	PA2
10	33.67	39.97	38.15	32.97	35.14	43.10	43.10	42.45	42.45	37.59	39.09	42.51	42.51
20	29.42	34.99	35.73	30.79	31.43	39.22	39.22	38.97	38.97	37.12	37.28	39.16	39.15
30	23.79	31.66	33.85	30.23	29.14	36.71	36.71	36.89	36.89	35.21	36.03	37.09	37.09
40	19.10	28.29	31.93	27.93	27.01	34.33	34.33	35.04	35.04	33.63	34.84	35.40	35.36
50	15.27	24.03	30.25	25.12	25.09	32.26	32.27	33.38	33.39	32.11	33.51	33.84	33.80
60	12.39	20.42	28.56	21.55	23.35	30.01	30.03	31.67	31.68	30.68	32.12	32.31	32.25
70	10.06	16.57	26.88	18.90	21.34	27.90	27.90	29.92	29.92	29.36	30.70	30.93	30.75
80	8.14	12.59	24.87	15.59	19.10	24.88	24.87	27.46	27.48	27.43	28.64	28.81	28.65
90	6.68	9.05	22.14	12.83	16.03	20.08	20.08	23.80	23.80	25.26	26.19	26.42	26.20

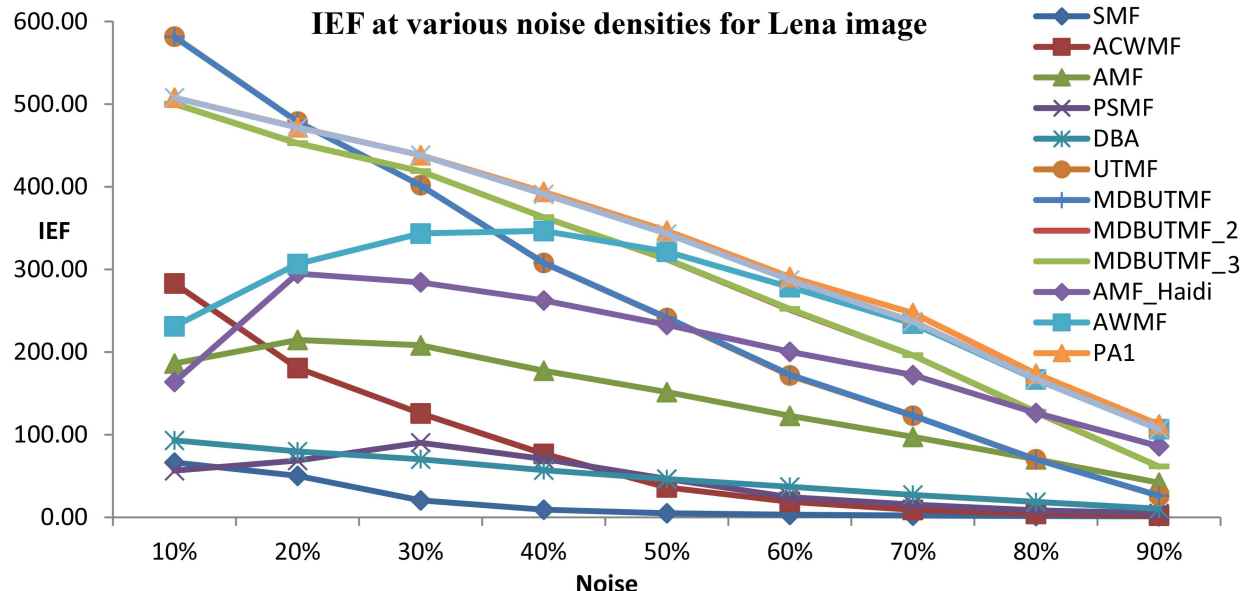


Fig. 12 Plot of IEF results given by various filters for Lena image at various noise densities

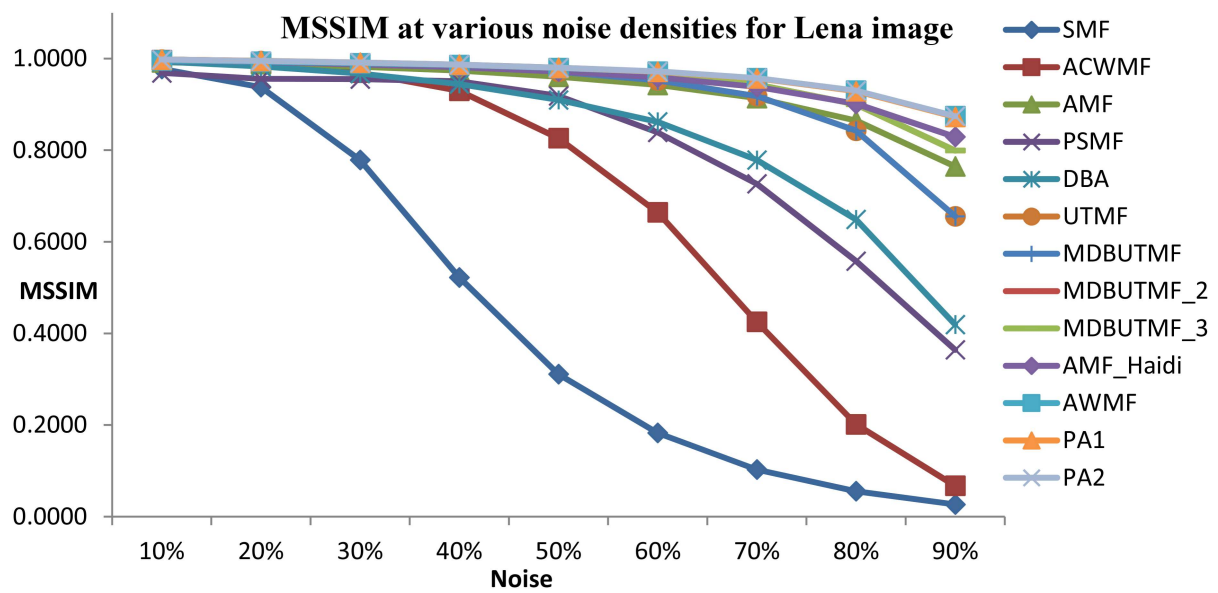


Fig. 13 Plot of MSSIM results given by various filters for Lena image at various noise densities

for all test images show that PA1 and PA2 give the highest scores for all noise densities >15%, whereas <15% noise density UTMF and MDBUTMF give the highest score. Figs. 12 and 13 show the IEF and MSSIM results given by the various filters at all noise densities for the Lena image. The IEF plot in Fig. 12 shows that MDBUTMF and UTMF have the highest score at 10% but the score declines gradually. At all other noise densities, PA1 and PA2 have the highest scores for all test images. The MSSIM plot in Fig. 13 shows that most of the filters have similar scores until 60%

noise density but above 60% noise density, PA1, PA2, and AWMF have the highest scores. Tables 6 and 7 show the EPrA and EPrR results given by the various filters at all noise densities for the Lena image. For all test images, PA2 gives the highest edge preservation ratio than all the other methods. PA1 gives similar results as PA2 for lower to medium noise densities. AWMF gives the second highest score at higher noise densities.

When the timing for execution taken in seconds by all the filters are compared as shown in Table 8, PA1 and PA2 consume

Table 6 EPRa results for the Lena image at all noise densities

Noise, %	SMF	ACWMF	AMF	PSMF	DBA	UTMF	MD BUTMF	MD BUTMF_2	MD BUTMF_3	AMF_Haldi	AWMF	PA1	PA2
10	0.744	0.916	0.870	0.881	0.866	0.930	0.930	0.931	0.931	0.888	0.899	0.930	0.930
20	0.686	0.848	0.834	0.830	0.771	0.887	0.887	0.898	0.898	0.855	0.876	0.902	0.902
30	0.583	0.767	0.777	0.767	0.663	0.827	0.827	0.847	0.847	0.789	0.834	0.855	0.855
40	0.464	0.669	0.719	0.662	0.553	0.758	0.758	0.802	0.802	0.732	0.802	0.813	0.814
50	0.382	0.536	0.655	0.525	0.436	0.676	0.676	0.738	0.738	0.667	0.764	0.769	0.769
60	0.339	0.414	0.584	0.384	0.322	0.556	0.556	0.653	0.653	0.580	0.708	0.705	0.715
70	0.317	0.308	0.492	0.230	0.248	0.405	0.405	0.535	0.535	0.484	0.642	0.621	0.646
80	0.318	0.246	0.387	0.083	0.184	0.266	0.266	0.399	0.401	0.349	0.519	0.490	0.519
90	0.314	0.232	0.269	0.022	0.187	0.169	0.169	0.255	0.255	0.202	0.379	0.336	0.378

Table 7 EPRr results for the Lena image at all noise densities

Noise, %	SMF	ACWMF	AMF	PSMF	DBA	UTMF	MD BUTMF	MD BUTMF_2	MD BUTMF_3	AMF_Haldi	AWMF	PA1	PA2
10	0.637	0.849	0.787	0.748	0.766	0.877	0.877	0.876	0.876	0.818	0.834	0.875	0.875
20	0.516	0.744	0.734	0.644	0.626	0.809	0.809	0.822	0.822	0.775	0.794	0.828	0.828
30	0.331	0.625	0.650	0.581	0.500	0.727	0.727	0.753	0.753	0.694	0.741	0.760	0.760
40	0.183	0.479	0.573	0.510	0.375	0.634	0.634	0.686	0.686	0.625	0.693	0.702	0.702
50	0.118	0.330	0.495	0.391	0.273	0.537	0.537	0.608	0.608	0.546	0.628	0.637	0.636
60	0.088	0.211	0.411	0.268	0.193	0.415	0.415	0.512	0.512	0.454	0.566	0.562	0.572
70	0.076	0.125	0.322	0.149	0.132	0.280	0.280	0.397	0.397	0.361	0.486	0.470	0.488
80	0.073	0.082	0.234	0.058	0.092	0.170	0.170	0.275	0.276	0.248	0.365	0.343	0.366
90	0.071	0.068	0.147	0.016	0.075	0.096	0.096	0.154	0.154	0.140	0.228	0.211	0.228

Table 8 Time taken in seconds for restoring Lena image at various noise densities by the various filters

Noise, %	SMF	ACWMF	AMF	PSMF	DBA	UTMF	MD BUTMF	MD BUTMF_2	MD BUTMF_3	AMF_Haldi	AWMF	PA1	PA2
10	11.02	42.95	14.40	42.07	4.92	5.74	5.51	5.24	9.47	3.20	71.21	1.89	1.93
20	11.00	42.99	16.97	43.21	5.07	6.44	6.60	6.30	10.58	4.28	51.78	3.47	3.53
30	10.76	43.18	14.77	50.62	5.35	7.60	7.73	7.29	11.79	6.34	42.19	5.06	5.36
40	10.85	42.37	14.50	51.96	6.08	8.61	8.82	8.22	12.41	8.29	37.67	6.69	6.73
50	10.84	41.65	15.77	53.09	6.12	9.78	9.94	9.33	13.41	13.54	32.02	8.38	8.40
60	10.80	41.64	20.36	54.55	6.59	10.74	11.20	10.28	14.72	17.31	32.20	10.24	10.45
70	10.74	41.67	21.84	55.89	6.95	11.77	12.31	11.31	15.54	23.63	31.25	12.92	12.50
80	10.79	41.58	31.51	58.65	7.46	12.98	13.58	12.28	16.29	32.92	33.34	16.83	14.69
90	10.79	41.57	65.89	59.45	7.51	14.56	15.23	13.15	17.35	59.09	42.20	24.61	20.83

considerably less time than all the adaptive filters. The proposed method requires only a minimum of one or two good pixels in the nearest neighbourhood for restoration. This criterion restricts the size of the adaptive filtering window to a minimum yielding faster execution time and lesser blurring effect. When their execution time is compared with the 3×3 filters, PA1 and PA2 consume less time than 3×3 filters until 40% noise density but >40%, the DBA, UTMF, and MDBUTMF variants take less time than all the other filters. However, they give poor restoration results than all the adaptive filters at higher noise densities. PA1 and PA2 take around 90% less time than the best performing adaptive filter AWMF for noise densities <50% and around 50% less time for noise densities >50%.

The proposed algorithms are also tested with bio X-ray images for analysing their performance in the presence of numerous black and white pixels. The proposed algorithms show similar performance for both standard grey-scale images and X-ray images in terms of PSNR, MAE, MSSIM, IEF, EPRa, and EPRr measures. Figs. 14–16 show the chest X-ray image restored by various filters at 90% salt and pepper noise. The proposed methods show good restoration results and PA2 gives the highest edge preservation ratio. In the case of execution time for X-ray images, PA1 and PA2 are faster than all adaptive filters. When their execution time is compared with 3×3 filters at lower noise densities, PA1 and PA2 run faster than DBA and MDBUTMF variants for X-ray images having smaller white or black regions, whereas DBA and MDBUTMF variants run faster than PA1 and PA2 for X-ray images with larger black or white regions. At larger white or black regions, the filtering window size of the proposed method reaches

its maximum, as it could not find enough good pixels in the neighbourhood, affecting its execution time.

Fig. 17 shows timing versus MAE plot of various filters for the Lena image corrupted with 90% noise density. It is found that for all standard test images at higher noise densities, 3×3 filters (SMF, DBA, UTMF, MDBUTMF variants) consume less time than adaptive filters where window size can be increased. However, the adaptive filters AMF, AWMF, AMF_Haldi, AWMF, PA1, and PA2 give better MAE scores at very high noise densities. PA1 gives the best MAE score among all the filters, whereas AWMF and PA2 give the second best MAE scores. PA1 and PA2 take considerably less time than all the adaptive filters.

4 Conclusion

In this paper, a fast and efficient adaptive and selective mean filter is proposed which removes high-density salt and pepper noise effectively than many existing state-of-the-art filters. Adaptive filters show better restoration results for images corrupted with high-density salt and pepper noise than 3×3 filters, but they consume more time. The proposed adaptive filter consumes considerably less time than the existing best adaptive filters for high-density salt and pepper noise removal, which is vital for their implementation in image acquisition devices.

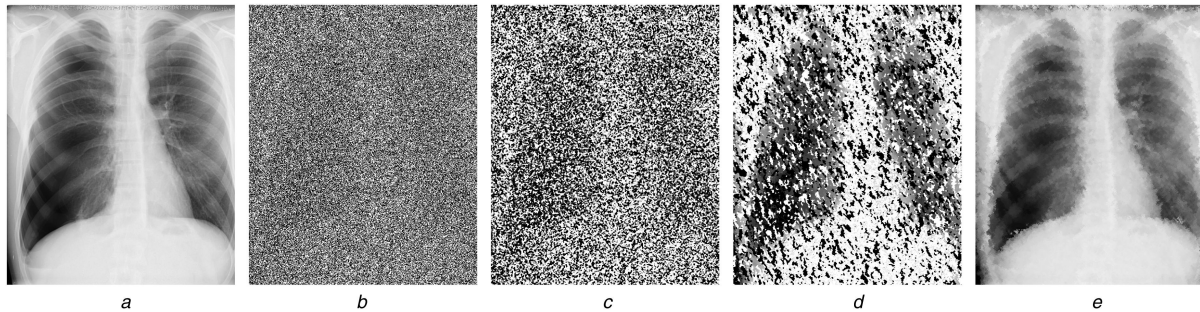


Fig. 14 Restored 500×612 chest X-ray images at 90% salt and pepper noise by various filters – part 1
(a) Original image, (b) Image with 90% salt and pepper noise. Image restored by, (c) SMF, (d) ACWMF, (e) AMF

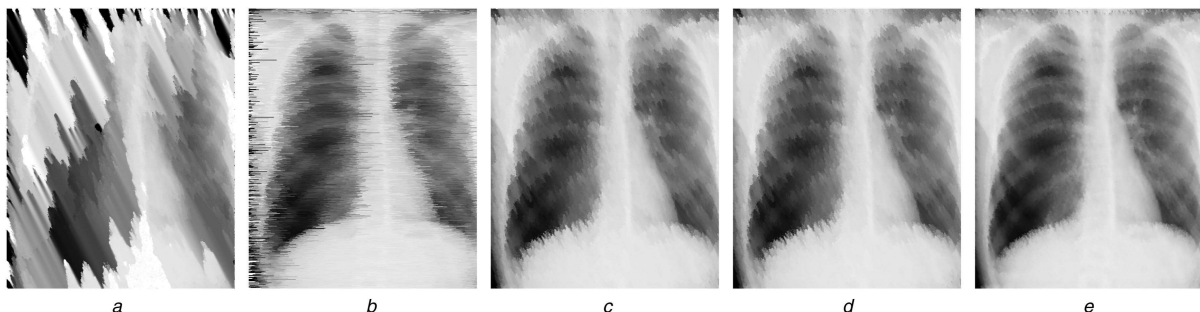


Fig. 15 Restored 500×612 chest X-ray images at 90% salt and pepper noise by various filters – part 2
(a) PSMF, (b) DBA, (c) UTMF, (d) MDBUTMF, (e) MDBUTMF_2

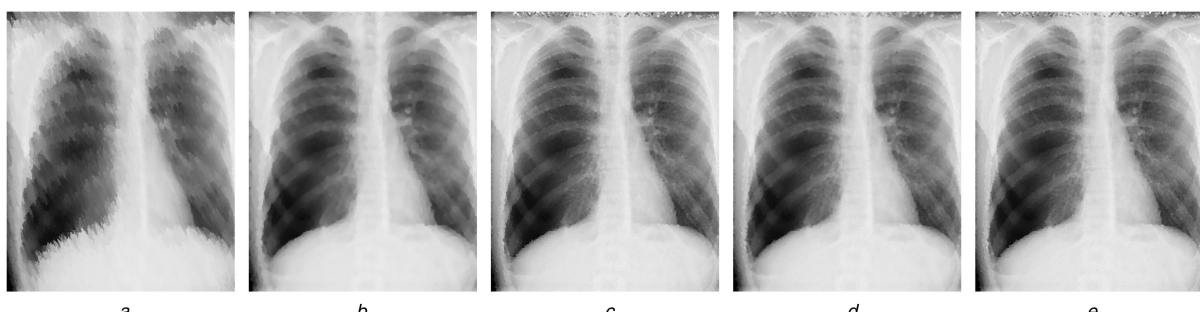


Fig. 16 Restored 500×612 chest X-ray images at 90% salt and pepper noise by various filters – part 3
(a) MDBUTMF_3, (b) AMF_Haidi, (c) AWMF, (d) PA1, (e) PA2

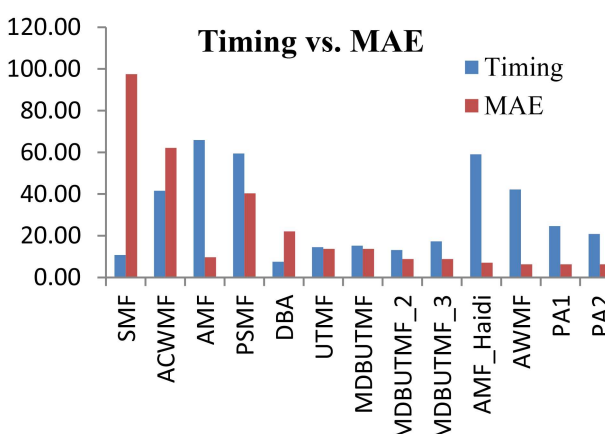


Fig. 17 Timing versus MAE plot for various filters for the Lena image corrupted with 90% noise density

5 References

- [1] Michael, A.C.: ‘Digital SLR astrophotography’ (Cambridge University Press, New York, 2007), ISBN 0-521-70081-7
- [2] Pitas, I., Venetsanopoulos, A.N.: ‘Nonlinear digital filters principles and applications’ (Kluwer Academic Publishers, Boston, 1990)
- [3] Sun, T., Neuvo, Y.: ‘Detail-preserving median based filters in image processing’, *Pattern Recognit. Lett.*, 1994, **15**, pp. 341–347
- [4] Wang, Z., Zhang, D.: ‘Progressive switching median filter for the removal of impulse noise from highly corrupted images’, *IEEE Trans. Circuits Syst. II*, 1999, **46**, pp. 78–80
- [5] Hwang, H., Haddad, R.A.: ‘Adaptive median filters: new algorithms and results’, *IEEE Trans. Image Process.*, 1995, **4**, (4), pp. 499–502
- [6] Chen, T., Wu, H.R.: ‘Adaptive impulse detection using center-weighted median filters’, *IEEE Signal Process. Lett.*, 2001, **8**, pp. 1–3
- [7] Srinivasan, K.S., Ebenezer, D.: ‘A new fast and efficient decision-based algorithm for removal of high-density impulse noises’, *IEEE Signal Process. Lett.*, 2007, **14**, pp. 189–192
- [8] Aiswarya, K., Jayaraj, V., Ebenezer, D.: ‘A new and efficient algorithm for the removal of high density salt and pepper noise in images and videos’. Second Int. Conf. Computer Modeling and Simulation, Sanya, Hainan, China, 2010, pp. 409–413
- [9] Esakkirajan, S., Veerakumar, T., Subramanyam, A.N., et al.: ‘Removal of high density salt and pepper noise through modified decision based unsymmetric trimmed median filter’, *IEEE Signal Process. Lett.*, 2011, **18**, pp. 287–290
- [10] Gupta, V., Gandhi, D.K., Yadav, P.: ‘Removal of fixed value impulse noise using improved mean filter for image enhancement’. IEEE Nirma University Int. Conf. Engineering, Ahmedabad, India, 2013
- [11] Chaitanya, N.K., Sreenivasulu, P.: ‘Removal of salt and pepper noise using advanced modified decision based unsymmetric trimmed median filter’. Int. Conf. Electronics Communication Systems, Coimbatore, India, 2014
- [12] Ibrahim, H., Kong, N.S.P., Ng, F.: ‘Simple adaptive median filter for the removal of impulse noise from highly corrupted images’, *IEEE Trans. Consumer Electronics*, 2008, **54**, (4), pp. 1920–1927
- [13] Zhang, P., Li, F.: ‘A new adaptive weighted mean filter for removing salt-and-pepper noise’, *IEEE Signal Process. Lett.*, 2014, **21**, (10), pp. 1280–1283
- [14] Veerakumar, T., Esakkirajan, S., Vennila, I.: ‘Edge preserving adaptive anisotropic diffusion filter approach for the suppression of impulse noise in images’, *AEU Int. J. Electron. Commun.*, 2014, **68**, (5), pp. 442–452
- [15] Song, Y.H., Han, Y.S., Oh, J.S., et al.: ‘Edge preserving impulse noise reduction’, *J. Imaging Sci. Tech.*, 2013, **57**, (6), pp. 60507-1–60507-8(8)

- [16] Wei, Y., Yan, S., Yang, L., *et al.*: ‘An improved median filter for removing extensive salt and pepper noise’, IEEE Int. Conf. Mechatronics and Control, Jinzhou, China, 2014, pp. 897–901
- [17] Kumar, R.R., Vasanth, K., Rajesh, V.: ‘Performance of the decision based algorithm for the removal of unequal probability salt and pepper noise in images’, IEEE Int. Conf. Circuit Power and Computing Technologies, Nagercoil, India, 2014, pp. 1360–1365
- [18] Dash, A., Sathua, S.K.: ‘High density noise removal by using cascading algorithms’. IEEE Fifth Int. Conf. Advanced Computing & Communication Technologies, Haryana, India, 2015, pp. 96–101
- [19] Beagum, S., Sathik, M.M., Hundewale, N.: ‘Improved adaptive median filters using nearest 4-neighbors for restoration of images corrupted with fixed-valued impulse noise’. IEEE Int. Conf. Computational Intelligence and Computing Research, Madurai, India, 2015, pp. 1–8
- [20] Wang, Y., Wang, J., Song, X., *et al.*: ‘An efficient adaptive fuzzy switching weighted mean filter for salt-and-pepper noise removal’, *IEEE Signal Process. Lett.*, 2016, **23**, (11), pp. 1582–1586
- [21] Wang, X., Shi, G., Zhang, P., *et al.*: ‘High quality impulse noise removal via non-uniform sampling and autoregressive modelling based super-resolution’, *IET Image Process.*, 2016, **10**, (4), pp. 304–313
- [22] Roig, B., Estruch, V.D.: ‘Localised rank-ordered differences vector filter for suppression of high-density impulse noise in colour images’, *IET Image Process.*, 2016, **10**, (1), pp. 24–33
- [23] Lin, P.H., Chen, B.H., Cheng, F.C., *et al.*: ‘A morphological mean filter for impulse noise removal’, *J. Display Tech.*, 2016, **12**, (4), pp. 344–350
- [24] Chen, C.L.P., Liu, L., Chen, L., *et al.*: ‘Weighted couple sparse representation with classified regularization for impulse noise removal’, *IEEE Trans. Image Process.*, 2015, **24**, (11), pp. 4014–4026
- [25] Bai, T., Tan, J.: ‘Automatic detection and removal of high-density impulse noises’, *IET Image Process.*, 2015, **9**, (2), pp. 162–172
- [26] ‘Image databases’. Available at http://www.imageprocessingplace.com/root_files_V3/image_databases.htm, accessed May 2017
- [27] ‘The National Library of Medicine presents Medpix’. Available at <https://medpix.nlm.nih.gov/home>, accessed May 2017
- [28] Yu, S., Li, R., Zhang, R., *et al.*: ‘Performance evaluation of edge-directed interpolation methods for noise-free images’. Proc. Fifth Int. Conf. Internet Multimedia Computing and Service, ACM, Huangshan, China, 2016, pp. 268–272